J. Synchrotron Rad. (2000). **7**, 301–306

Synchrotron beam test with a photon-counting pixel detector

Ch. Brönnimann,[a] S. Florin,[b] M. Lindner,[b]* B. Schmitt[a] and C. Schulze-Briese[a]

[a]*Swiss Light Source, Paul Scherrer Institute, CH-5232 Villigen-PSI, Switzerland, and* [b]*Physikalisches Institut der Universität Bonn, Nussallee 12, D-53115 Bonn, Germany.* *E-mail: lindner@physik.uni-bonn.de*

(*Received 27 March 2000; accepted 20 June 2000*)

Synchrotron beam measurements were performed with a single-photon-counting pixel detector to investigate the influence of threshold settings on charge sharing. Improvement of image homogeneity by adjusting the threshold of each pixel individually was demonstrated. With a flat-field correction, the homogeneity could be improved. A measurement of the point spread function is reported.

Keywords: pixels; charge sharing; flat-field corrections; photon counting.

1. Introduction

Protein crystallography is an important application of synchrotron radiation that takes advantage of the new developments in radiation sources such as the Swiss Light Source (SLS) (Bengtsson *et al.*, 1997; Joho *et al.*, 1994). At the SLS protein crystallography beamline a minigap in-vacuum undulator will produce high-brightness synchrotron radiation. The high brightness leads to the need for new detector systems providing high readout speed for short dead times, to minimize radiation damage of sensitive biological crystals.

The most promising detector type for this application are single-photon-counting pixel detectors (Brönnimann *et al.*, 2000). They provide a large dynamic range, high rate capability, low noise performance, very fast data readout, sufficient spatial resolution and can be assembled to large area detectors (Barna *et al.*, 1995; Beauville *et al.*, 1997; Fischer *et al.*, 1999). A 2k × 2k system with 200 μm × 200 μm pixels is under development at the SLS.

However, there has been concern regarding charge-sharing effects in pixel detector systems, leading to problems with their suitability as detectors for protein crystallography. In this application a very homogeneous response of the detector to the incident radiation is necessary in order to determine the relative intensities of reflections with high accuracy. Areas between the pixels with a higher or lower efficiency owing to charge sharing would lead to problems.

Therefore the influence of basic detector parameters on charge sharing between pixels and on the overall detector homogeneity has been investigated.

2. Experimental set-up

All measurements were performed at the optics beamline (BM5) at the European Synchrotron Radiation Facility (ESRF) in Grenoble, France.

2.1. *Beamline*

ESRF bending magnets provide a beam of divergence 6 mrad × 0.2 mrad and a critical energy of 20.4 keV. The beam size at BM5 is ∼60 mm × 5 mm. Energy is selectable with a monochromator in the range 8–25 keV. The beam was collimated with motorized slits to 10 μm × 10 μm. A second slit system was positioned at a distance of ∼1 m from the first one, directly in front of the detector, to block slit scattering. The settings of the slits were monitored with an NaI scintillator, which was also used to determine the beam profile from a slit scan (Fig. 1).

2.2. *Detector*

Since a bump-bonded SLS pixel chip (Brönnimann *et al.*, 2000) is not yet available, the MPEC chip (Fischer *et al.*, 1998) was used for the present measurements. It is well characterized (Fischer *et al.*, 1999) and provides the same functionality as the SLS chip, except for radiation hardness and pixel geometry.

The MPEC chip is divided into 12 columns and 63 rows of identical pixels of size 433.4 μm × 50 μm. Each pixel contains the complete pixel readout electronics including

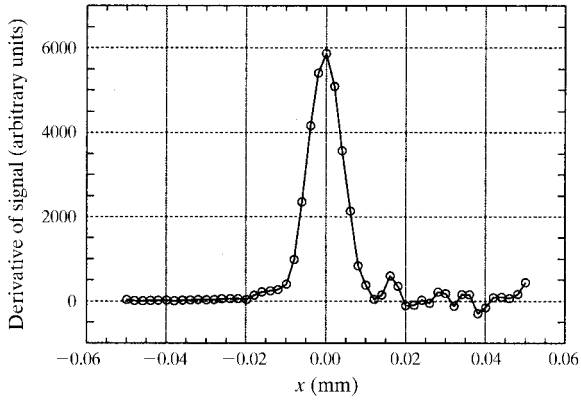

Figure 1
Beam profile at 12 keV obtained with a slit scan.

an amplifier for positive input polarity, a discriminator which detects an event above threshold, a 15-bit counter, and test and masking capabilities.

The discriminator is controlled by two threshold voltages: a global threshold for all pixels and a correction voltage, stored on a capacitor in each pixel to compensate threshold variations on the chip. This feature is extremely important for a homogeneous response of the detector, as will be shown in §3.

The counter is realized as a linear feedback shift register (Fischer *et al.*, 1996) with dynamic flip-flops and can be read out serially by connecting all counters of a column. All 12 columns are then read out in parallel.

The large dynamic range of $2^{15} - 1$ is given by the counter size and can be increased by multiple readout of the detector during data acquisition.

The sensor bump-bonded onto the electronic chip is a 300 µm-thick silicon p^+n diode array, which has adequate quantum efficiency in the low energy range used here (99% at 8 keV and 52% at 15 keV).

The chip behaviour with sensor has been studied previously (Fischer *et al.*, 1999). The noise of 135 $\pm$ 41 e^- allowed threshold settings of below 2000 e^-. After adjustment, the threshold variation over the complete chip measured with a threshold scan (Fischer *et al.*, 1999) was 38 e^-.

2.3. *Readout system*

The chip was wire-bonded onto a printed circuit board connected to a Blue Board test system (Silicon Solutions GbR, Rosenstrasse 7–9, D-50678 Köln, Germany) providing all voltages and currents for the chip and transferring the digital signals to the PC. The refresh of the dynamic counters is performed by a free programmable gate array on the Blue Board; the refresh of the threshold adjustment is performed by the PC in a background task running independently from the measurement program.

3. Results

3.1. *Homogeneity*

The detector homogeneity is one of the most important quality criteria for protein crystallography as well as for medical imaging.

A homogeneity measurement was performed, irradiating the detector uniformly. For this, a fluorescent crystal consisting of a glass plate with an amorphous Ge-doping was put into the beam, producing a homogeneous field of energy 12 keV.

The measurement was performed with 120 V sensor bias voltage and thresholds set to 2000 e^-. To investigate the influence of the threshold adjustment, the measurement was performed with and without adjustment. The total exposure time was 33 min.

For the homogeneity studies, the border pixels were excluded in order to eliminate the effects of a sensor problem reported by Fischer *et al.* (1999).

In Fig. 2 the histogram of the count rates is shown with and without threshold adjustment. With adjustment, the average counts per pixel was 5640 with a standard deviation of 155 (Fig. 2*b*). This should be compared with Fig. 2(*a*) showing the same measurement without threshold adjustment. The gain in homogeneity owing to the threshold adjustment is clear.

To further investigate the influence of the threshold on the count rates in the pixels, the count rate is plotted *versus* the threshold in Fig. 3. As expected, there is a strong negative correlation visible, *i.e.* pixels with a higher threshold have lower count rates.

To further improve the homogeneity a flat-field correction was performed. The efficiency map of the detector has been calculated from the first half of the data set and then applied to the second half. The result after applying the correction map is compared with the homogeneity without efficiency correction in Fig. 4. The flat-field correction reduced the standard deviation in sensitivity from 2.77% to 1.89%.

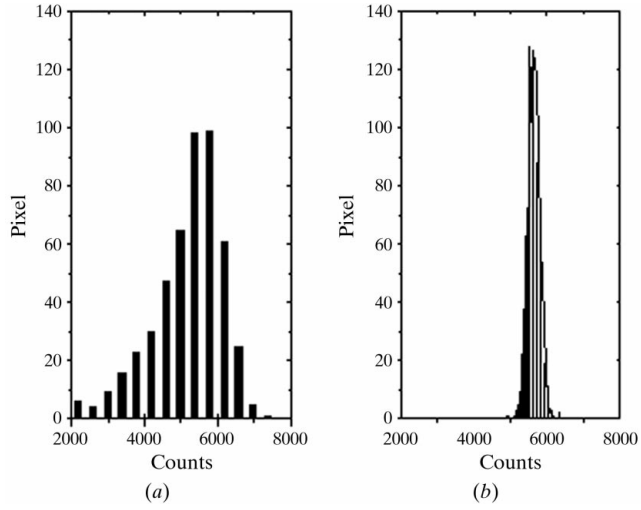

Figure 2
Count-rate histograms (*a*) without and (*b*) with threshold adjustment (events = 1–500; σ = 156 counts). The improvement by the adjustment is obvious.

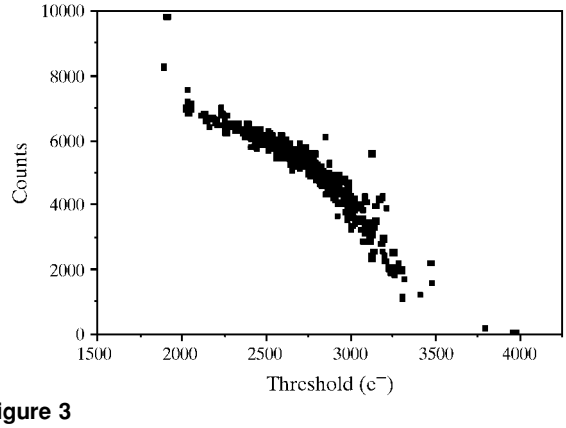

Figure 3
Count rate *versus* threshold, without adjustment. The negative correlation is obvious.

The image of the uniformly exposed detector with efficiency correction is shown in Fig. 5. The homogeneity is very good over the complete chip; even at the border the response improved significantly.

It should also be mentioned that a comparison of the first and second half of the data set (Figs. 2 and 4) shows that the threshold adjustment and thus the image homogeneity is stable in time. In any case, the threshold adjustment values were calculated before the test beam and used for all measurements, which proves their long time stability.

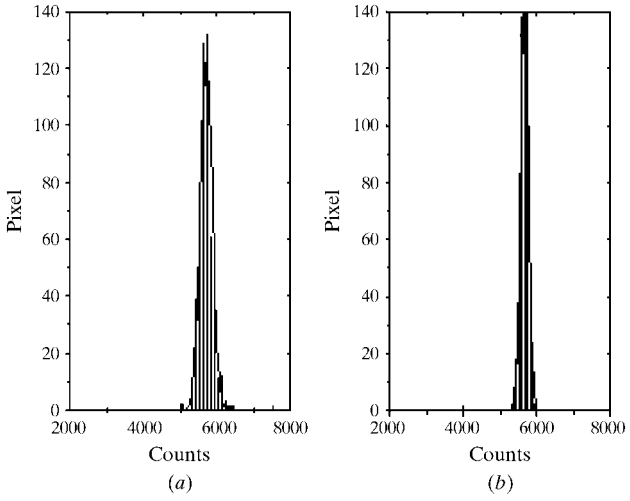

Figure 4
Count-rate histograms (*a*) with adjusted thresholds only (events = 501–1000; σ = 158 counts) and (*b*) with an additional efficiency correction (events = 501–1000; σ = 107 counts). The efficiency correction improves the homogeneity.

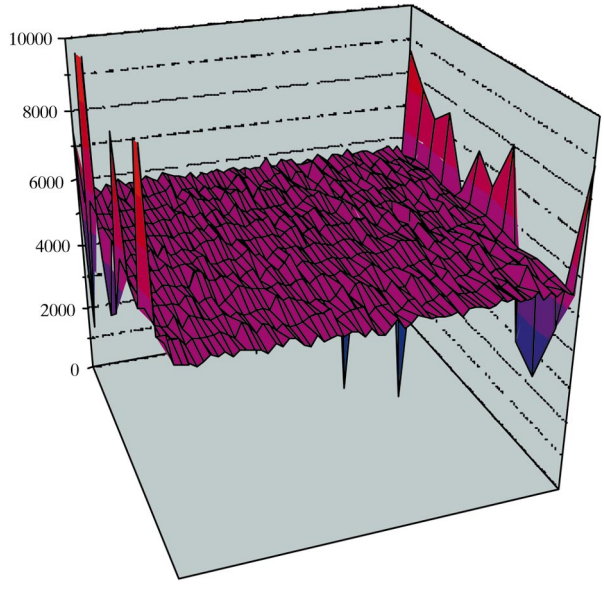

Figure 5
Uniform exposure of the detector with adjusted thresholds and efficiency correction. Only very rare pixels have problems.

3.2. *Point spread function*

In Fig. 6 the profile of the 10 μm × 10 μm beam recorded with the pixel detector is compared with that taken with a scintillator. With the pixel detector, the beam was centred on the pixel and the profile was taken in a single image. To achieve the point spread function with the scintillator, which provides only one-dimensional information, the beam was scanned in 50 μm steps. As can be seen, the full width at 1% maximum is still 50 μm with the pixel detector.

3.3. *Charge sharing*

Charge sharing between the pixels was measured by scanning the detector across the beam in steps of 5 μm along the 50 μm pixel direction with various threshold settings, beam energies and detector bias voltages. For all scans the counts in each pixel position as well as the sum of all pixels are plotted as a function of the beam position.

In the ideal case we expect that X-rays impinging exactly between two pixels should deposit the half charge generated by the photon in each pixel. Owing to this charge sharing between neighbouring pixels, a reduced efficiency between the pixels for a threshold higher than half the beam energy occurs, and *vice versa*, *i.e.* for a threshold below half the beam energy, a higher count rate between the pixels is expected, because now the charges on both pixels can be above the threshold. For a threshold of exactly half the beam energy, we expect an optimal response.

Fig. 7 shows the scans with a variation of the threshold settings. The beam energy is fixed at 18 keV which leads to a charge deposition in the detector of 5000 e^-. The thresholds have been set to 3000 e^-, 2500 e^- and 2000 e^-. With a threshold at half the beam energy, the effect of charge sharing is significantly reduced.

Next the beam energy was varied with a fixed threshold setting of 2000 e^- and a bias voltage of 120 V. Fig. 8 shows the same effect as observed for the threshold variation: for a low beam energy (8 keV) the half value is below the

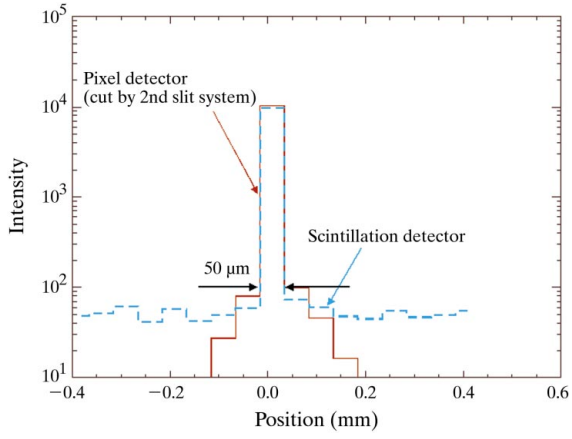

Figure 6
Beam profile of a 10 μm × 10 μm beam measured with the MPEC pixel detector (solid line). A reference measurement was performed with a scintillation counter (dashed line).

threshold leading to an inefficiency between the pixels. For half the beam energy close to the threshold as shown in the centre panel of Fig. 8, the inefficiencies due to charge sharing are again minimized. With a high beam energy we see a higher count rate between the pixels as expected (Fig. 8, bottom).

The overall intensity variations in the three plots in Fig. 8 result from variations in the beam alignment for the three monochromator positions and not from the detector absorption differences for the three energies.

A scan with the detector tilted towards the beam was also performed. The tilt angle was set to 15° (Fig. 9) and 30° (Fig. 10). In both cases the influence of charge sharing is significantly reduced because, for a given position of the detector, only a reduced fraction of the X-rays convert in the zone between the pixels. Fig. 9 can be compared directly with Figs. 11 and 8 showing the improved homogeneity gained by tilting the detector.

The decreasing total count rate over the scan results from an absorption of the X-rays by the housing of the detector, which has an entrance window covered by a 100 µm Al foil. When the detector was tilted above a certain angle, the beam hit the housing and the intensity was attenuated.

A two-dimensional scan of the region at the corner of four pixels was performed for two threshold settings at a beam energy of 12 keV and a detector bias of 120 V. It is

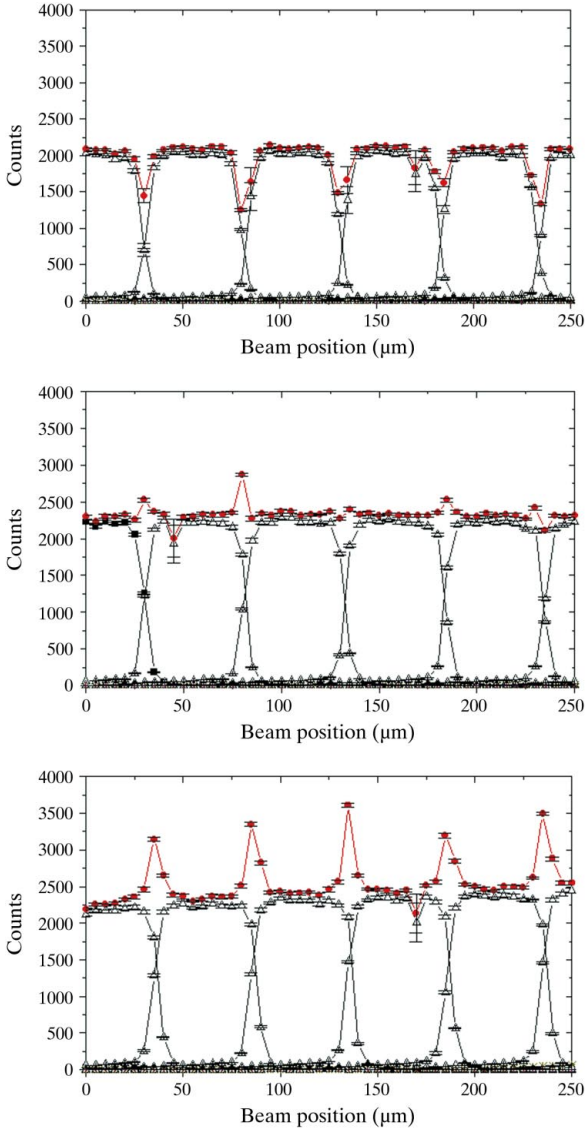

Figure 7
Scan with an 18 keV beam. The threshold has been set to 3000 e^- (upper plot), 2500 e^- (middle) and 2000 e^- (bottom). For 2500 e^- (half the beam energy) the effect of charge sharing is minimized.

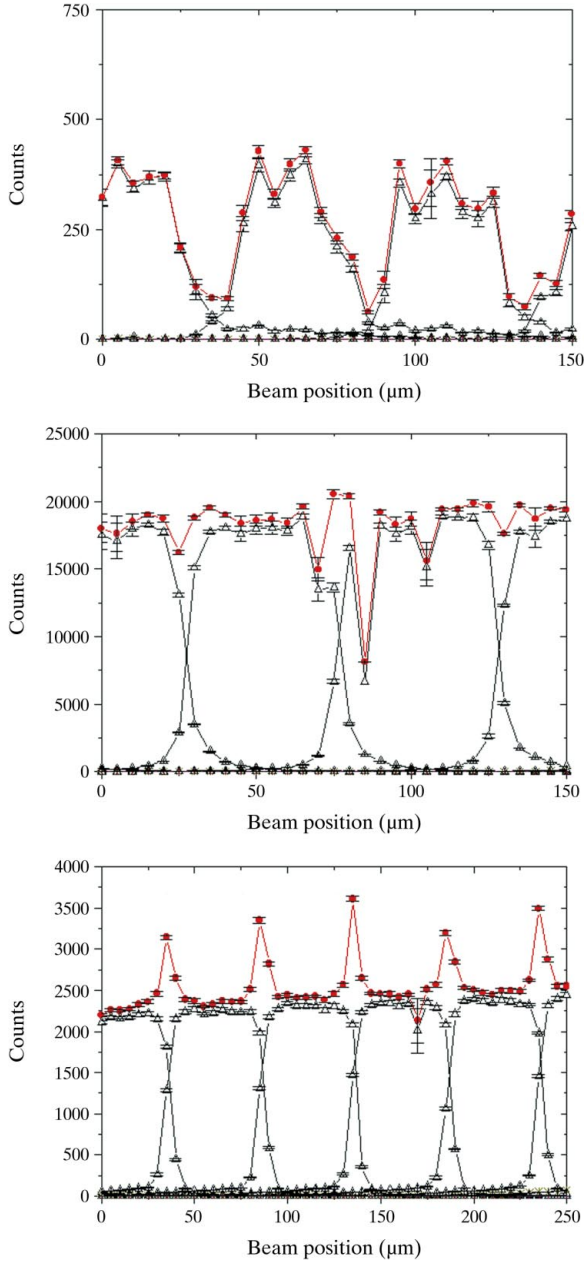

Figure 8
Scan with a threshold of 2000 e^- and a detector bias of 120 V. The beam energy has been set to 8 keV (upper plot), 12 keV (middle) and 18 keV (bottom). The two diverting data points are caused by an instability of the detector.

seen that, in the pixel corners, charge sharing occurs between more than two pixels so that there are some unavoidable inefficiencies in the area of four adjacent pixels (Figs. 11 and 12). However, it was shown that this problem can be reduced by operating the sensor with a higher bias voltage, because the higher electric field in the sensor increases the charge-carrier drift velocity and this reduces the spread of the charge distribution.

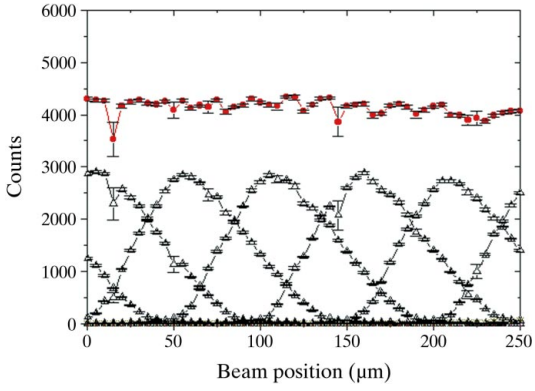

Figure 9
Scan with a 15° tilt angle, 12 keV beam energy and 2000 e^- threshold. There are no visible pixel-to-pixel inefficiencies.

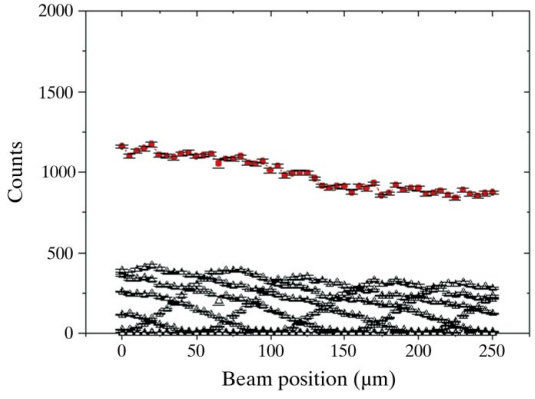

Figure 10
Scan with a 30° tilt angle, 12 keV beam energy and 2000 e^- threshold.

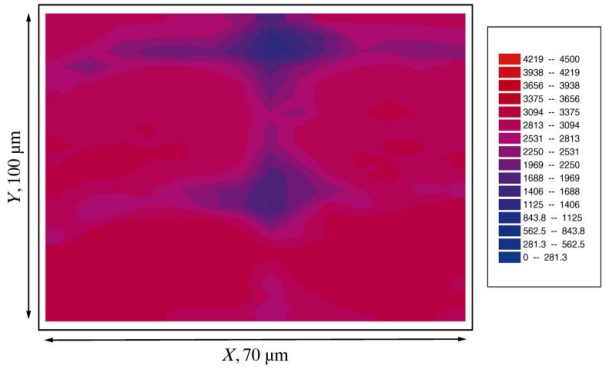

Figure 11
Two-dimensional scan of a pixel corner with a threshold set to 2000 e^-. Inefficiencies occur mainly in the pixel corners.

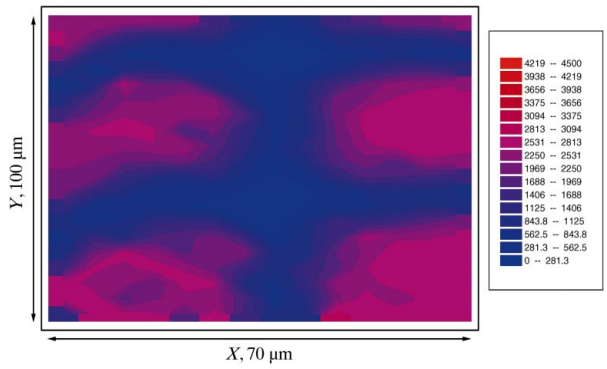

Figure 12
Two-dimensional scan of a pixel corner with a threshold set to 3000 e^-. Owing to the high threshold setting there are additional inefficiencies between the pixels.

4. Summary

It has been shown that the influence of charge sharing on the efficiency between the pixels can be reduced by setting the threshold to half the beam energy. Therefore a low-noise detector with a low threshold setting (below 2000 e^-) is necessary. However, this will be difficult to achieve for low beam energies, *i.e.* below 12 keV. Small areas of inefficiency will remain at the corners of the pixels.

When the detector is tilted towards the beam, the effects of charge sharing vanish independently of the threshold settings. Since the diffracted X-rays from a protein crystal will rarely hit the detector perpendicularly, we do not expect the average response to suffer from false counting effects.

The improvement in image homogeneity by the individual adjustment of the discriminator thresholds has also been demonstrated. This is one of the most important features of a single-photon-counting detector for protein crystallography.

The further improvement in homogeneity owing to a flat-field correction is promising. However, for a large detector the uniform exposure could be difficult to achieve.

The measured point spread function shows the superiority of a counting pixel detector with a width at 1% of the maximum equalling the pixel dimension.

In summary, a single-photon-counting pixel detector was shown to have promising characteristics for synchrotron beam experiments.

We would like to thank the ESRF beamline support group for providing the beam time for these tests, and the staff (Cyril Ponchut, Heinz Grafsma and Anna Puig) for their generous help in all questions concerning the beamline.

References

Barna, S. L., Shepherd, J. A., Wixted, R. L., Tate, M. W., Rodricks, B. & Gruner, S. M. (1995). *Proc. SPIE*, **2521**, 301–309.

Beauville, E., Beche, J.-F., Cork, C., Douence, V., Earnest, T., Millaud, J., Nygren, D., Padmore, H., Turko, B., Zizka, G., Datte, P. & Xuong, N.-H. (1997). *Nucl. Instrum. Methods*, A**395**, 429–434.

Bengtsson, J., Joho, W., Marchand, P., Milhaupt, G., Rivkin, L. & Streun, A. (1997). *Nucl. Instrum. Methods*, A**404**, 237.

Brönnimann, Ch. *et al.* (2000). *Nucl. Instrum. Methods*. Submitted.

Fischer, P. (1996). *Nucl. Instrum. Methods*, A**378**, 297–300.

Fischer, P., Hausmann, J., Overdick, M., Raith, B., Wermes, N., Blanquart, L., Bonzom, V. & Delpierre, A. (1998). *Nucl. Instrum. Methods*, A**405**, 53–59.

Fishcher, P., Hausmann, J., Helmich, A., Lindner, M., Wermes, N. & Blanquart, L. (1999). *IEEE Trans. Nucl. Sci.* **46**(4), 1070–1074.

Joho, W., Bengtsen, J., Marchend, P., Rivkin, A. & Streun, A. (1997). *Proceedings of EPAC96*, Vol. 1, pp. 685–687. Bristol: Institute of Physics.